Cement and Concrete Research 41 (2011) 1167–1176

Contents lists available at ScienceDirect

Cement and Concrete Research

journal homepage: http://ees.elsevier.com/CEMCON/default.asp

Effects of mixing energy on technological properties and hydration kinetics of grouting mortars

Keisuke Takahashi [a,*], Thomas A. Bier [b], Torsten Westphal [b]

[a] UBE Industries, Ltd. Seavans North Bldg, 1-2-1, Shibaura, Minato-Ku, Tokyo 105-8449, Japan
[b] Institut für Keramik, Glas- und Baustofftechnik der TU Bergakademie Freiberg, Germany

ARTICLE INFO

Article history:
Received 19 February 2011
Accepted 19 July 2011

Keywords:
Mixing energy
Rheology (A)
Hydration products (B)
Shrinkage (C)
Admixture (D)

ABSTRACT

During slurry preparation, effects of certain phenomena on fluidity and hardening characteristics of cement-based grouts have been reported. Deterioration of fluidity and hardening will affect the slurry performance, quality of workmanship and result in subsequent structural defects. There has been little research conducted on the effects of mixing energy during slurry preparation which has focused on the reasons or mechanisms for changes in characteristic properties. This work describes and measures the effects of several mixing parameters on properties of grouting materials, such as fluidity, hardening characteristics, shrinkage, heat of hydration, ion elution and crystallographic structure using X-ray diffraction and SEM. The results indicate that long mixing processes cause deterioration in fluidity and setting properties. These observations can be explained by acceleration in hydration kinetics and changes in microstructures and subsequent changes in dispersion states due to different mixing durations.

1. Introduction

Grouting materials are self-flowable mortars. Some construction methods involving earthquake resistant design and sewage drain rehabilitation use grouting materials to fill and reinforce gaps and cavities [1]. For these applications grouts need to have good fluidity and stable hardening characteristics to ensure their optimum placement and flawless integrity of construction. Continuous mode equipment and discontinuous mode equipment such as batch type mixers and concrete mixers are usually used to produce grouting slurries. Fernandesa et al. reported that slurry characteristics differed with the equipment types due to differences in mixing capacities [2]. It has been reported that certain phenomena during slurry preparation and pumping conditions can adversely affect fluidity and hardening characteristics. The deterioration of fluidity and hardening will cause filling problems and subsequent structural defects. Very little research on the influence of mixing energy during slurry preparation and pumping has focused on the reason or mechanisms for changes in characteristic properties. Sugiyama and Uomoto suggested that differences in dispersion conditions, depending on dispersing agent, as well as differences in the form of hydrates, affected micro-pore structures and strength of cement pastes [3]. Martinez-Ramirez et al. described slurry preparation using continuous mode equipment and suggested that slurry preparation influenced some results such as apparent density, strength and shrinkage [4]. Baskoca et al. investigated relationships between mixing time and slump loss and strength using a concrete mixer [5]. Tsutsui and Ouchi examined relationships between pumping distance and fluidity of concrete [6].

All this research points to the fluidity and hardening of the slurry being affected by the mixing energy during the slurry preparation and pumping, which is dependent on the equipment used and the composition of grouting materials. This investigation into the reasons for the mechanisms of change in characteristic properties is therefore a significant one. The results of this work should consequently ensure ideal placement of grouting and perfect, integral construction.

The effects of several mixing parameters on properties of grouting materials such as fluidity, hardening characteristics, shrinkage, heat of hydration, and ion elution are described and measured using X-ray diffraction (XRD) and scanning electron microscopy (SEM). Our objective is to evaluate whether the long mixing processes cause deterioration of fluidity and setting properties. These observations can be explained by acceleration in hydration kinetics, changes in microstructures and subsequently changes in dispersion states due to different mixing durations.

2. Experimental

2.1. Materials

The grouting materials consist of cement, aggregate and admixture.

* Corresponding author.
E-mail addresses: akaherudasen2000@yahoo.co.jp (K. Takahashi), Thomas.Bier@ikgb.tu-freiberg.de (T.A. Bier), Torsten.Westphal@ikgb.tu-freiberg.de (T. Westphal).

0008-8846/$ – see front matter © 2011 Elsevier Ltd. All rights reserved.
doi:10.1016/j.cemconres.2011.07.005

- Cement: Ordinary Portland cement CEMI 32.5R type by Lafarge Co., Germany.
- Aggregate: Local silicious sand with a maximum grain size of 1.0 mm
- Admixture: Polycarboxylic ether (PCE) super plasticizer Melflux2651F by BASF Co., Germany.

2.2. Methods

Most of grouts or mortars are mixed for 2 or 3 min to obtain optimal fluidity, however, since there is no standard working practice for the duration of the mixing, both poorly mixed (less than 1 min) and excessively mixed slurries occur on construction sites all over the world. Therefore, to cover this range of real-world mixing scenarios, the time periods for mixing the slurry were predetermined at 1 min (less mixing), 2 min (normal mixing), 5 min and 7 min (excessive mixing).

Prior to the testing, cement, sand and PCE were pre-mixed (dry and hand mixing) in the proportions as shown in Table 1 and subsequently mixed with 180 g water in a beaker for a maximum of 7 min at 700 rpm with a chemical stirrer (Heidolph Co. products). Composition A was a basic formulation used in all tests. Composition B was used to observe the effects of dispersion performance on slurry characteristics. The PCE dose was increased from 0.80 g to 1.10 g in compositions B and D. A cooling bath was used for compositions C and D to monitor the effects of temperature increase on slurry characteristics. The bath was set at 15 °C in order to inhibit the elevation of slurry temperature. All tests were performed in a 20 °C constant temperature room.

Fluidity, dimensional stability, setting time, compressive strength, hydration kinetics, ion elution, X-ray diffraction and EDX-SEM of the grouting materials were measured. Every test was repeated more than three times in the same conditions.

2.2.1. Fluidity

Fluidity was evaluated by flow value and J_{14}-funnel efflux time. The flow value was measured using a 50 Φmm*100 mm mini-slump cone, based on EN 12706 and JIS R 5201. The spread of the slurry on a flow plate was determined and the J_{14}-funnel efflux time was measured based on JHS 312. The slurry was set into a funnel immediately after mixing. In each test, the time until the whole slurry flowed through was measured as the J_{14}-funnel efflux time.

2.2.2. Dimensional stability

For the dimensional stability measurement, a shrinkage drain was used. The measurement of shrinkage or expansion took place in a mould with 25-cm length and a rectangular cross section of 38 mm by 60 mm. The shrinkage or expansion was monitored continually during the 24 h after mixing. The measurements were tested with and without a polyethylene cover.

2.2.3. Setting time and compressive strength

Setting time and compressive strength were measured based on EN 196. Samples were cured in water and tested at time intervals of 1, 3, 7 and 28 days.

2.2.4. Hydration kinetics

Calorimetric tests as an index of hydration kinetics were carried out using the isothermal conduction calorimeter of a triple type produced by J. Kuzel [7]. The rate of heat evolution was monitored for 24 h.

2.2.5. Ion elution

To measure ion concentrations, the sampling method conformed with the tank-leaching test method. The slurry was mixed for the predetermined period of time, then diluted 1:10 with water, filtered with a 0.45 μm membrane-filter and tested with SPECTRO FLAME S (ICP atomic emission spectrometer). The sampling was conducted immediately after mixing and after 4 h had elapsed.

2.2.6. EDX-SEM

EDX-SEM images were measured by using a ESEM XL 30 FEG (FEI) environmental scanning electron microscope with field emission. The hydration process of samples was terminated after 1 day of curing.

2.2.7. X-ray diffraction

X-ray diffraction patterns were measured with a X'PERT Pro MPD PW 3040/60 diffractometer from Panalytical with a fast detector in order to check continuously the hydrate formation after mixing. A diffraction pattern was acquired every 5 min during the first 24 h of hydration.

2.2.8. Mixing energy

The mixing energy (defined as the torque during slurry mixing) was measured using the software Watch&Control2000 (Heidolph Co. products). The value of torque was recorded once every second.

3. Results

3.1. Fluidity and slurry temperature

Table 2 shows the fluidity of slurry compositions A–C (slurry A–C) as a function of mixing time. The flow value was measured immediately after mixing (t_0) and 5 min after filling the flow cone (t_5). The fluidity worsened with an increase in mixing time, however, it improved with the cooling bath and an increase in the super plasticizer dose.

Fig. 1 shows slurry temperature for compositions A and C as a function of mixing time. The temperature of slurry A increased as the mixing period became longer. The temperature of slurry C stayed constant at 20 °C due to the cooling bath.

3.2. Dimensional stability

Figs. 2 and 3 show early shrinkage of slurry A after 1, 2, 5 and 7 min mixing as a function of time with and without cover, respectively. In comparing these, it is evident that, shrinkage in uncovered slurries always exceeded shrinkage in covered slurries. The shape of shrinkage curves between Figs. 2 and 3 is also very different. Whereas the curves in Fig. 2 show shrinkage only after an initial slight expansion, the curves in Fig. 3 show shrinkage from the onset and this is more pronounced compared to Fig. 2. All shrinkage curves without cover show a *distinct kink* in the beginning when the curves decrease steeply. Regardless of the absence or presence of a cover, shrinkage increased as the length of mixing time increased. Fig. 4 shows the difference in shrinkage between slurry A and B without cover as a

Table 1
Proportions of the grouting materials (unit; g).

	Cement	Sand	PCE	Cooling bath
A	430	570	0.80	Without
B			1.10	Without
C			0.80	With
D			1.10	With

Table 2
Fluidity of slurry A–C as a function of mixing time.

	Slurry A				Slurry B	Slurry C	
Mixing time (min)	1	2	5	7	7	2	7
Flow value (t_0) (mm)	249	249	165	138	252	251	168
Flow value (t_5) (mm)	241	220	153	127	240	249	161
J_{14}-funnel efflux time (sec)	6.5	6.6	7.9	9.1	6.4	6.4	7.7

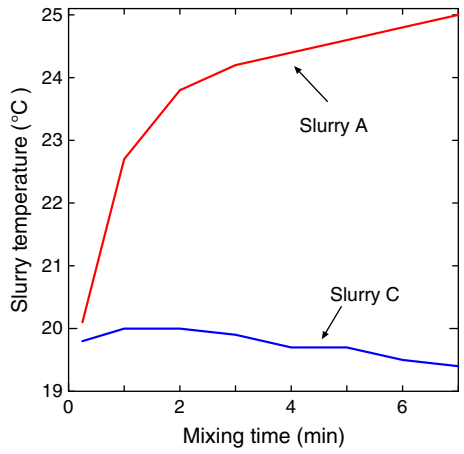

Fig. 1. Slurry temperature for compositions A and C as a function of mixing time.

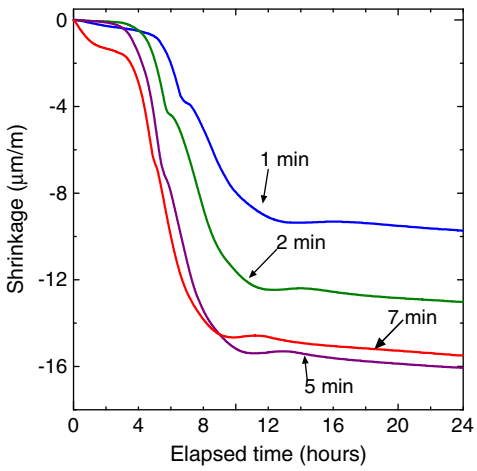

Fig. 3. Early shrinkage of slurry A without cover as a function of time.

function of time for slurries mixed for 7 min. The slurry with improved dispersion (B) shows less shrinkage. Fig. 5 shows shrinkage differences between slurry A and C without cover as a function of time mixed for 2 and 7 min. Slurries mixed with the cooling bath (C) exhibit less shrinkage. The different behaviour seems more pronounced at the beginning of the measurement i.e. before the kink.

3.3. Setting time and compressive strength

Setting times and compressive strength data of slurries A and B are shown in Table 3. With longer mixing times, the initial and final set shortened and early compressive strengths increased. In contrast, every sample exhibited approximately equal compressive strengths after 7 and 28 days. With an increased dose of super plasticizer, setting time was extended.

3.4. Hydration kinetics

Heat evolution rates of slurry A as a function of time are plotted in Fig. 6 for mixing periods of 1, 2, 5 and 7 min. With increasing mixing time, the start of massive precipitation (beginning of accelerated period) was advanced and the second peak of the heat evolution curves increased. Fig. 7 represents heat evolution curves 0 through 2 h as a function of time (initial dissolution). The initial dissolution rate at a given time became more pronounced as mixing periods became longer. Fig. 8 shows the differences between heat evolution rate of slurry A and B as a function of time for a mixing period of 7 min. The slurry with improved dispersion (B) retarded hardening, however, it did not decrease the second peak value. Fig. 9 demonstrates time-dependent differences of the heat evolution rate between slurry A and C — for 2-min and 7-min mixing periods. The heat evolution curves do not change irrespective of whether there is a cooling bath, but clearly do change as a function of the mixing time period.

3.5. Ion elution

Table 4 shows ion concentrations in slurries A and B mixed for different time periods that were detected immediately after mixing and after 4 h. The ion concentration increased immediately after mixing when the mixing period became longer. Ca^{2+} ion elution increased significantly. This acceleration of ion elution is caused solely by a lengthening of the mixing period since static curing for 30 min after mixing does not cause an increase of ion elution [8]. However, after 4 h, both sample A mixed for 2 min and sample A mixed for 7 min, exhibited approximately equal ion concentrations. This indicates that longer mixing time periods enhance early ion dissolution. In contrast to slurry A, slurry B (with improved dispersion due to PCE dose) showed delayed ion dissolution.

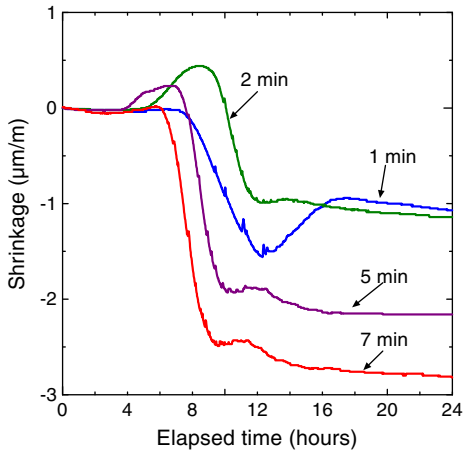

Fig. 2. Early shrinkage of slurry A with cover as a function of time.

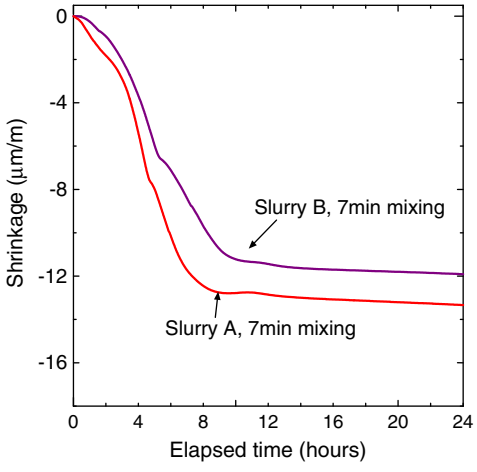

Fig. 4. Difference in shrinkage between slurries A and B without cover as a function of time.

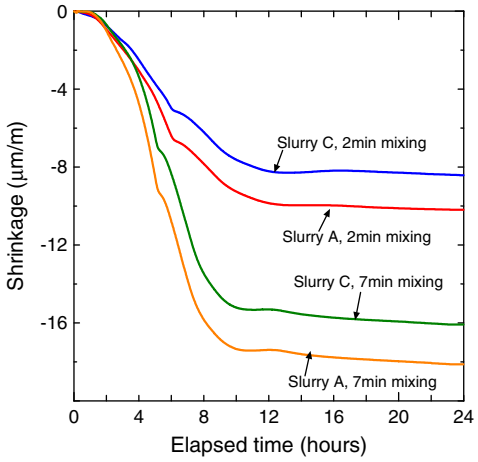

Fig. 5. Shrinkage differences between slurries A and C without cover as a function of time.

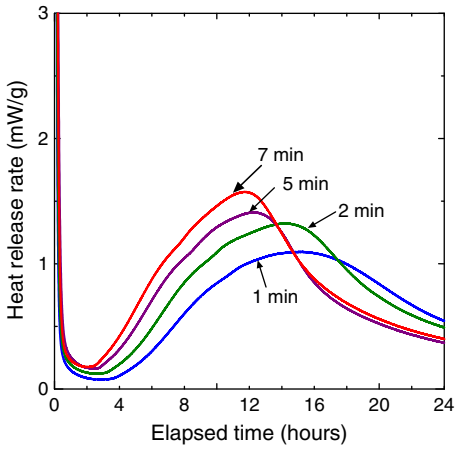

Fig. 6. Heat evolution rate of slurry A as a function of time.

3.6. EDX-SEM

To determine differences in structures and crystal conditions, SEM images were observed for fracture cross sections on hardened samples of slurry A mixed for 1 min and 7 min. Figs. 10 and 11 show relatively large, plate-like hydrates and Figs. 12 and 13 show needle-like hydrates. Table 5 shows the chemical compositions using EDX microanalysis on cross sections (Figs. 10–13). The hydrate from C_3S can be identified as portlandite (CH) due to its plate-like shape and high Ca proportion (Table 5). The hydrates from the interstitial phase (C_3A and C_4AF) can be identified as calcium aluminate silicate hydrate and ettringite because of their proportions. With longer mixing times, the shape of hydration product crystals became well pronounced and enlarged, although Ca content in CH decreased and SO_3 and Al content in ettringite increased.

3.7. X-ray diffraction

To clarify relationships between the differences of hydrates and mixing, X-ray tests were carried out. At first, the hydrating samples of slurry A were measured in situ, starting immediately after mixing to follow changes in phase composition. X-ray peaks of quartz, anhydrite, ettringite, CH and alite had been observed. After the in-situ measurements were taken, the hardened samples were pulverized for quantitative powder XRD. Although there was no significant difference in phase composition for powdered samples, in-situ XRD showed different CH peak intensities for each sample [9]. CH peak intensities were measured at (001)-reflection (18.00°2θ) and (101)-reflection (34.10°2θ). Fig. 14 represents the (001)-intensity of CH as a function of time in each sample. Fig. 15 represents the (101)-intensity of CH as a function of time in each sample.

The intensities of the CH reflections generally increased with measurement time due to the progressing hydration. The intensities also generally decrease with increasing mixing time. This effect was more pronounced for the (001)-reflection than for the (101)-reflection.

Table 3
Setting times and compressive strength data of slurries A and B.

		Slurry A				Slurry B
Mixing time (min)		1	2	5	7	7
Setting time (h:min)	Initial set	6:10	5:50	5:10	4:45	5:05
	Final set	8:00	7:45	7:05	6:45	7:00
Compressive strength (N/mm^2)	1 day	20.0	22.0	23.6	23.4	22.4
	3 days	33.7	40.2	41.9	40.2	40.8
	7 days	47.8	50.9	51.2	49.7	49.9
	28 days	57.2	58.8	59.1	56.8	57.2

3.8. Mixing energy

Fig. 16 shows the mixing energy for slurries A–D as a function of mixing time. Table 6 shows the integrated values of the mixing energy as a function of mixing time. The mixing energy increased to a maximum value immediately after padding samples into water and then it decreased. Compared to slurry A, the mixing energy of slurry B (with improved dispersion) decreased. Compared to slurry A and B, the mixing energy of the cooled slurry (C and D) decreased.

4. Discussion

4.1. Temperature increase

These findings on setting time, compressive strength and heat evolution rate resemble the characteristics of concrete cured at different temperature conditions as reported in Suto and Akiba [10]. Their study compared properties at 20 °C and 35 °C, and reported the following changes as temperature increased:

1) Hydration commences earlier in the accelerated period.
2) The second peak value of the hydration heat evolution rate is increased.
3) Setting time is advanced.

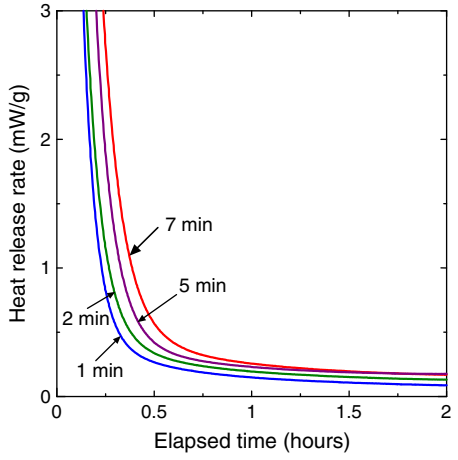

Fig. 7. Heat evolution curves during initial 2 h of mixing as a function of time.

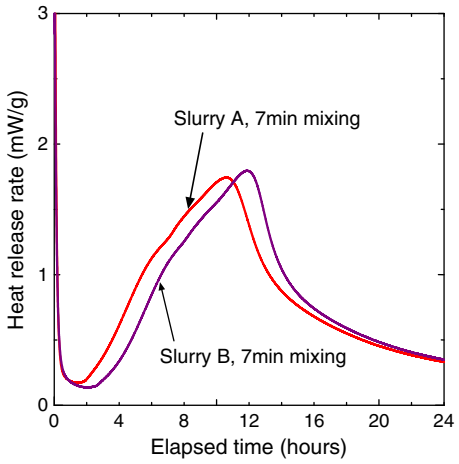

Fig. 8. Difference of heat evolution rate between slurries A and B as a function of time.

4) Early strength is developed, although long-term strength is decreased.

This paper proposes that acceleration in hydration processes causes these phenomena. The rate of hydration increases as temperature increases and generally follows the Arrhenius equation [11]. This equation defines the relationship between temperature and reaction rate. Fig. 1 shows that slurry temperature increased to 25.0 °C during the 7 min of mixing. Logically this temperature increase could possibly affect hydration acceleration. To determine the effects of temperature increase, heat evolution rate, shrinkage and fluidity were measured while inhibiting the increase of slurry temperature. Comparing slurry A and C, Fig. 9 indicates that heat evolution curves were not dependent on cooling but only on mixing time. This indicates that hydration is accelerated due to the duration of mixing and not due to rises in the temperature.

4.2. Mechanism of hydration acceleration

There are some general reviews concerning the early hydration mechanism. The reactions of C_3S begin immediately upon wetting. Heat is released by dissolution of C_3S but the dissolution rate decelerates very quickly during the initial dissolution period. There are several hypotheses which explain this deceleration.

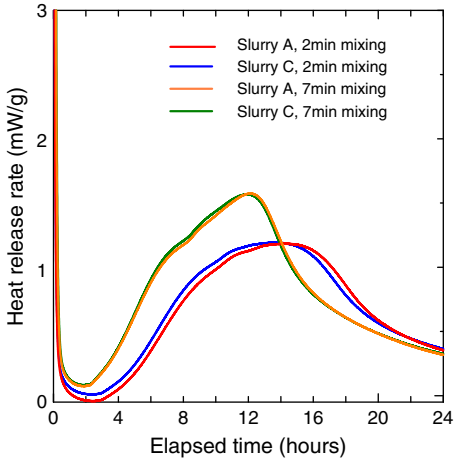

Fig. 9. Differences of heat evolution rate between slurries A and C as a function of time.

Table 4
Results of ion concentration (unit; ppm).

	Slurry A				Slurry B	
Mixing time	2 min		7 min		7 min	
Settling time	Immediately	4 h	Immediately	4 h	Immediately	4 h
Na^+	239	303	245	273	255	240
K^+	3429	3922	3674	3884	3796	3447
Ca^{2+}	3069	6224	3839	6204	3191	4418

1. Metastable layer hypothesis: The deceleration is caused by the rapid formation of a continuous but thin metastable layer of a calcium silicate hydrate phase [12], which effectively passivates the surface by restricting its access to water, or restricts diffusion of detaching ions away from the surface [13]. Schweitzer et al. measured the hydrogen depth profile at and below the surface using nuclear resonance reaction analysis and interpreted that the layer extends progressively deeper into the solid [14]. The rate of C_3S dissolution in the period of initial reaction would continue to be rapid up to much higher solution concentrations of calcium and silicates if not for the formation of the passivating hydrate layer [15].
2. Slow dissolution step hypothesis: Nonat et al. [16–18] explained the deceleration as being based on a steady state balance between slow dissolution of C_3S and initially slow growth of CSH. When the solution exceeds a maximum supersaturation with respect to CSH, CSH nucleates very rapidly on C_3S surfaces and begins to grow slowly because of its initially low surface area. Growth of CSH causes the silicate concentration in solution to decrease and the Ca: Si molar ratio in solution to increase. Within minutes, a steady state condition is set up in which the solution is supersaturated with respect to CSH (the formation of an electrical layer) and subsequently the dissolution slows down (onset of the induction period). More recently Juilland et al. [19] reported that dissolution systems are primarily limited by the ion diffusion through the electrical layer and become progressively limited by surface reactions [20] as the undersaturation of the solution decreases with time.

Gartner et al. [21] listed some proposed mechanisms for the beginning of the accelerated hydration rate after the induction period and reported that the hydration rate (the rate of C_3S dissolution) is controlled by the rate of nucleation and growth, and not the other way around. Both the metastable layer hypothesis and the slow dissolution step hypothesis can explain this dependence of the dissolution rate on nucleation and growth. As a logical extension of the metastable layer hypothesis, nucleation and growth of stable CSH happen at the end of the induction period and are rate-controlling during the acceleration

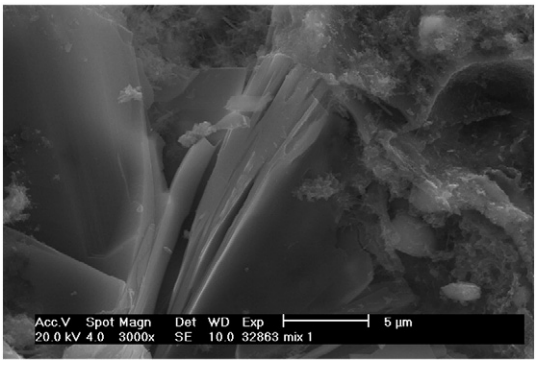

Fig. 10. SEM image of plate-like hydrates in sample mixed for 1 min.

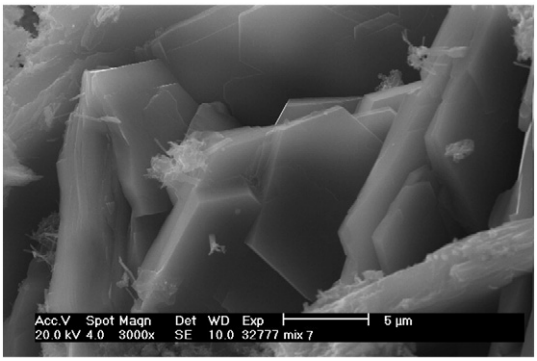

Fig. 11. SEM image of plate-like hydrates in sample mixed for 7 min.

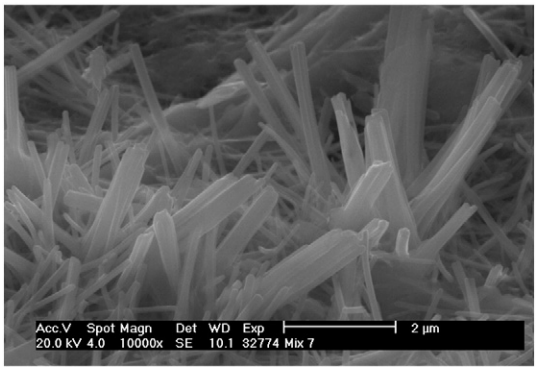

Fig. 13. SEM image of needle-like hydrates in sample mixed for 7 min.

period as a metastable protective layer of hydrate becomes chemically unstable and exposes the high-solubility C_3S. According to the slow dissolution step hypothesis, during the induction period, the solution is progressively enriched in calcium and hydroxides, causing to approach the critical supersaturation of CH. At the end of the induction period the hydrates grow at a nearly exponential rate. During the acceleration period, both CSH and CH are present and their increasing rates of growth continuously remove ions from solution which must be replenished by further dissolution of C_3S.

C_3A also reacts very quickly with water to form calcium hydroaluminates. According to Holly et al. [22], the hydrated products form a more or less permeable layer on the C_3A surface that limit the transport of water and ions during initial reaction. Skalny et al. [23] considered the adsorption of sulphate ions on C_3A. The sulphate ions therefore would block the active sites of the dissolution and would contribute to the decrease of the dissolution rate of C_3A. The sulphate ions are continually consumed by the reaction to form ettringite and therefore a quasi-stationary state is established. After the exhaustion of the sulphate ions in solution, the next period begins, when the renewal of C_3A dissolution and the growth of AFm occur [24].

D. Dollimore reported that mixing could influence the rate of heat evolution and this would consequently also affect setting time and compressive strength development [25]. R. Ylmén suggested that different mixing methods influence the formation states of CSH gels at early hydration stages [26]. From these reports, the mechanism of hydration acceleration can be assumed as follows: CSH and ettringite precipitate on cement grains immediately after addition of water. With extended mixing times more surfaces of cement particles become exposed to dissolution and/or reaction (increase in the active sites of dissolution and/or reaction). This is caused by destruction of protective superficial layers on cement gains. More specifically, the mixing procedure could disturb the electrical layer, or could scrape off the primary hydrates, or could destroy the passivating hydrate layer on the surface, or could cause all phenomena together. The destruction to the area of the layers is restored by further dissolution and precipitation. The consecutive repetition of destruction and of restoration increases the dissolution rate and accelerates the continuous nucleation and growth of hydrates such as CSH and ettringite. The solution is enriched in calcium and hydroxides, however sulphate ions in the solution are consumed with increasing speed. As a consequence, the transition to the induction period is prolonged and the induction period is shortened.

Fig. 7 indicates that in the initial dissolution period the rate of heat evolution became increased as mixing time became longer, which means that dissolution of anhydrous phases was accelerated. Comparing Ca^{2+} ion concentration between 2 min and 7 min (Table 4), it can be observed that Ca^{2+} ion elution immediately after mixing increases as mixing time becomes longer. This represents an increase of dissolution rate immediately after mixing with extended mixing time. This increase of the initial dissolution could be caused by the consecutive repetition of destruction and of restoration of the superficial layers. The increase of the dissolution prolongs the transition to the induction period. Fig. 6 shows that massive hydration commenced earlier and the second peak value of the heat evolution rate became increased as the mixing time became longer. This indicates an increase of the dissolution rate and subsequent change in the growth of hydrates in the acceleration period.

Hydrates are formed on/around the surface in the acceleration period and the formation of the hydrates in deceleration period is hindered due to the lack of space. Bishnoi et al. [27] proposed that a loosely-packed CSH fills a large fraction of the microstructure during early hours of hydration and the further development of its microstructure occurs due to an increase in its packing. Thereby the hydration rate in deceleration period is dependent on the formation of hydrates in acceleration period. Suto and Akiba [10] observed the following for the massive hydration of CSH on samples with an accelerated initial reaction: Outer CSH gels grow roughly and coarsely but inner CSH gels grow densely during the accelerated period. The

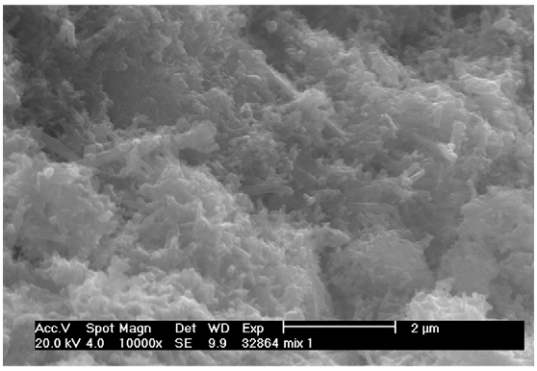

Fig. 12. SEM image of needle-like hydrates in sample mixed for 1 min.

Table 5
Chemical compositions using EDX on cross sections (Figs. 10–13) (unit; mol%).

	Fig. 10	Fig. 11	Fig. 12	Fig. 13
CaO	93.3	86.4	64.1	54.0
SiO_2	4.6	5.8	24.4	21.2
SO_3	1.2	1.5	6.1	10.5
Al_2O_3	0.4	1.5	3.3	9.7
MgO	0.5	3.8	1.0	2.8
Fe_2O_3	0.0	0.4	0.4	1.2
K_2O	0.0	0.6	0.7	0.5

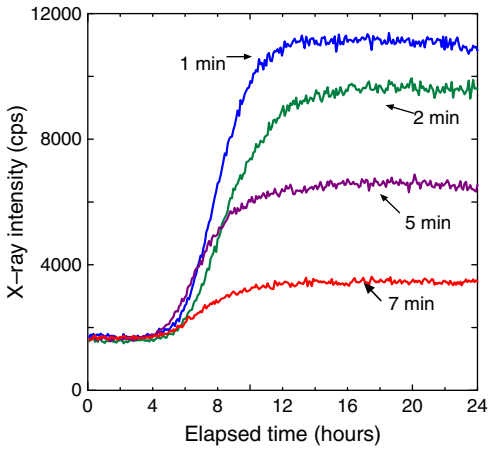

Fig. 14. (001)-intensity of CH as a function of time.

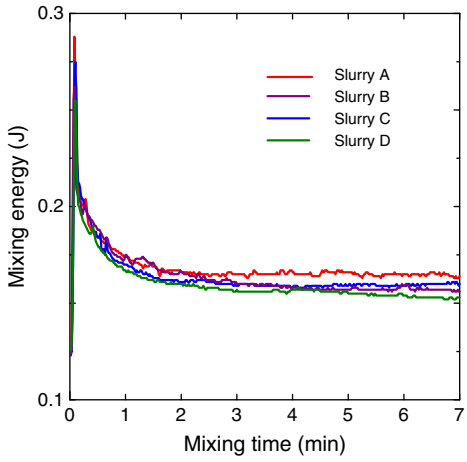

Fig.16. Mixing energy for slurries A–D as a function of mixing time.

outer gels progressively form inhomogeneous microstructures, however, for the inner gels, ion dissolution is inhibited because of their density. This could cause a decrease of heat evolution rate in the long term. All SEM images revealed that the cement grain structures became coarse, pronounced and enlarged as mixing time became longer. The changes in microstructure are considered to result from a different formation process of the inner/outer CSH during the acceleration period and a more homogeneous, but not necessarily a denser or more concentrated distribution of nucleation sites with extended mixing time.

4.3. Fluidity

Fluidity deterioration can be explained by the formation of hydrates, or by insufficient adsorption of super plasticizer, or by both phenomena occurring together. In the absence of super plasticizers, Hallal et al. reported that fluidity of cement pastes is related to hydration of cement [28]. Hanehara and Yamada suggested that fluidity deterioration is attributed to the large production of ettringite from the interstitial phase [29]. As mentioned above, extended mixing causes the increase of particle surfaces by destruction of the protective superficial layer, which leads to additional super plasticizer adsorption. Super plasticizers adsorb onto the hydrates such as calcium hydroxide nuclei and the initial hydration products of tricalcium aluminate [30]. This adsorption can retard hydration and disperse cement particles due to electrostatic repulsions and steric hindrances [31]. From these reports, it is conceivable that the large amount of hydrates, provoked by the lengthened mixing, does change the adsorbed amount of super plasticizer, thereby worsening the fluidity.

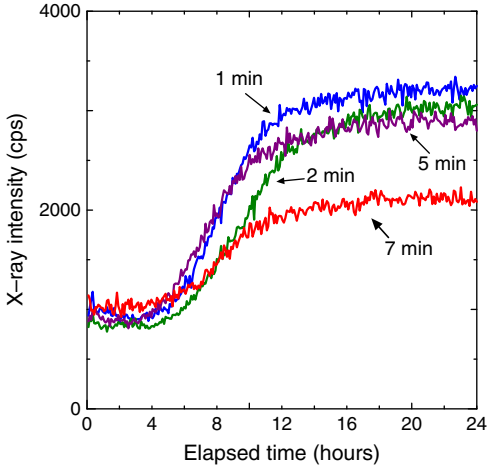

Fig. 15. (101)-intensity of CH as a function of time.

In order to substantiate this idea, two slurries with different doses of super plasticizer (slurries A and B) and a mixing time of 7 min are compared. Tables 2 and 3 show that fluidity was improved and setting and hardening were retarded with an increased super plasticizer dose. Table 4 shows that Ca^{2+} ion elution was delayed. In contrast to Fig. 6, heat evolution curves in Fig. 8 show a basic parallel shift in the case of increased plasticizer dose, whereas for a constant plasticizer dose and different mixing times, the curves changed profile and intersected each other.

The following can be deduced from these results. For slurry A active super plasticizer in water adsorbs onto hydrates on the surface. Both the adsorbing active super plasticizer and the hydrates are being scraped off by the mixing action. By removing hydrates with adsorbed plasticizer, less plasticizer will be available for further adsorption and this removed plasticizer becomes “inactive”. Destruction of the superficial layers leads to acceleration of Ca^{2+} ion elution and further hydrate formation. The active super plasticizer in water adsorbs onto the additional surfaces again. The repetition of adsorption and of abrasion reduces the active super plasticizer concentration in water and worsens fluidity. Nevertheless, hydration is not retarded because the available super plasticizer is not sufficient to adsorb onto all remaining hydrates. For slurry B the active super plasticizer in water similarly adsorbs onto the hydrates. Nonetheless, fluidity is not worsened and hydration is retarded because enough super plasticizer is available to adsorb onto the newly created surfaces hydrates. The delayed Ca^{2+} ion elution corroborates this.

In comparing slurries A and C, an improvement of fluidity was observed with the cooling bath. As mentioned above, the hydration

Table 6
Integrated values of the mixing energy as a function of mixing time (unit; J).

		Slurry A	Slurry B	Slurry C	Slurry D
Mixing time (min)	1	11.4	11.3	11.2	10.9
	2	21.5	21.4	21.0	20.6
	3	31.4	31.2	30.7	30.1
	4	41.3	40.7	40.2	39.5
	5	51.3	50.2	49.8	48.8
	6	61.1	59.6	59.3	58.1
	7	71.0	69.1	68.9	67.3

rate was not dependent on slurry temperature. This suggests that there is no difference in the amount of hydrates between slurry A and C. This also suggests that fluidity deterioration in this case is linked to temperature increase. H. Kato reported the adsorption of super plasticizer increased as the temperature of cement paste became elevated [32]. In the case of slurry C, it therefore, could be considered that the adsorption rate of super plasticizer is reduced. Even after the repetition of adsorption and abrasion, the amount of active super plasticizer in water is still enough to maintain fluidity.

4.4. Dimensional stability

Shrinkage in slurries that were covered and at a constant temperature corresponds to autogenous shrinkage and is largely influenced by hydration. Shrinkage in slurries that were uncovered and at constant temperature is a superposition of autogenous and evaporation shrinkage [33]. It is largely influenced by physical mechanisms such as fluidity and mobility of water in and out of the pore structure and the material. A comparison of shrinkage with and without cover (Figs. 2 and 3) represents that evaporation shrinkage is much larger than autogenous shrinkage in these slurries. Although there is increasing shrinkage in both slurries as mixing time becomes longer, the former (shrinkage with cover) indicates the relationship with changes of hydration. That is to say, the point of time when the curves change from slight expansion to shrinkage indicates the onset of the structuring process by massive hydration. As the mixing time becomes longer, hydration is accelerated and subsequently structuring occurs earlier, followed by increased autogenous shrinkage.

For measurements of uncovered slurries (Fig. 3), the beginning of structuring is signalled by a kink in the shrinkage curve. Both in plastic and solid states, the total amount of shrinkage of slurries without cover always exceeds shrinkage with the cover. The kink indicating the beginning of setting, however, shows up earlier as mixing time becomes longer. The pre-kink area corresponds to the plastic state and it is an indicator that shrinkage is dependent on fluidity and consistency of the slurry. The post-kink area corresponds to solid state and it is an indicator that shrinkage is dependent on hydration and the mobility of water moving in and out of pore structure and material [34]. As for the influence of pore structures, Bentur et al. [35] reported that the shrinkage during the solid state increased as pore volume of 30 nm or less increased. The pore volume of 30 nm or less is defined as a fine capillary pore space and gel pore space.

A comparison of slurries A and C (Fig. 5) reveals more pronounced differences in shrinkage, however, the appearance of the kink and the post-kink shrinkage influenced by hydration was very similar for slurries A and C that were mixed for the same length of time. The post-kink area corresponds more to the solid state and shrinkage dependents on hydration. Therefore, the post-kink shrinkage did not change with or without cooling, because massive hydration did not change. In the same way, longer mixing accelerated the massive hydration for slurry A and the shrinkage in the post-kink area increased as a function of the mixing time. The pre-kink shrinkage, however, depends more on physical characteristics of the slurry. Fluidity is improved with the cooling bath. As a consequence, the shrinkage is reduced (cf. Fig. 5). Reduction of pre-kink shrinkage is also observed with decreasing mixing time for slurries A and C. Comparing slurry A with B, Fig. 4 shows that not only the post-kink shrinkage but also the pre-kink shrinkage was decreased with the higher dose of super plasticizer, because fluidity was improved and hydration accelerated.

4.5. X-ray diffraction

The intensities of CH decreased with increasing mixing time. Regarding these results, four things could be considered. Firstly, it could be assumed that the hydrates decrease with longer mixing times. However, this assumption contradicts hydration acceleration interpreted above. Secondly, it could be assumed that there are some differences in structures and crystal conditions. Thirdly, preferred orientation on the surface of the measured sample could be hypothesized. As a fourth consideration, the samples develop a layered structure with CH precipitated preferably in the top layer, and this layered structure is more pronounced for shorter mixing time. The third and the fourth considerations may complement one another. Depending on sample conditions, the penetration depth of X-rays is less than 1 mm. Platy shaped CH crystals formed on the surface would result in disproportionately high peak intensities, especially for CH (001) reflections. Fig. 17 demonstrates clearly the preferred orientation, where the ratio of the two evaluated CH peaks at 18.00° (001) and 34.10° (101) is plotted. Theoretically, the ratio should be smaller than 1. The measured ratio approaches the theoretical value only for samples mixed for 7 min.

To study further the intensity decrease, SEM images (Figs. 18 and 19) with EDX analysis (Table 7) of the top surfaces for two mixing regimes were taken after 24 h. Figs. 20 and 21 show Ca and Si mapping images of a cross section by EDX. In Figs. 18 and 19 the dark points in the right-hand pictures are CH. Visually, there seems to be more CH on the upper surface of the sample for the shorter mixing time. Figs. 20 and 21 represent the differences in dispersion of Ca and Si around 100 μm from the upper surface. At the top of the images a surface layer is visible, indicating that the amount of Ca is higher in slurries mixed for 1 min than those mixed for 7 min. On the other hand, the amount of Si is lower in slurries mixed for 1 min than those for 7 min. These results support the idea of a surface film becoming thinner as mixing time becomes longer. It is generally agreed that if this film becomes thinner, water is easy to evaporate in the hardening process. If evaporation becomes more pronounced, the plastic or pre-kink shrinkage increases. This finding is in good correlation with the obtained shrinkage results.

With the above-mentioned X-ray and SEM results, it appears to be evident that hydrates are dispersed more homogeneously as mixing time becomes longer. This more homogeneous distribution of hydrates is considered to result from a more homogeneous distribution of water and nucleation sites. Shorter mixing time allows the formation of a surface layer with increased water content. This surface layer is the preferred place for CH precipitation. Furthermore, this surface layer provides the space to develop the pronounced preferential orientation of the forming CH crystals. Longer mixing times provide more homogeneous slurries with less pronounced surface layers. Therefore, decreased peak intensities and reduced preferential orientation of CH are observed.

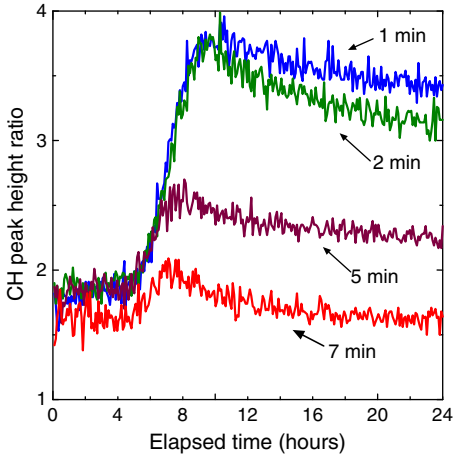

Fig. 17. XRD peak height ratio for CH intensities as a function of time.

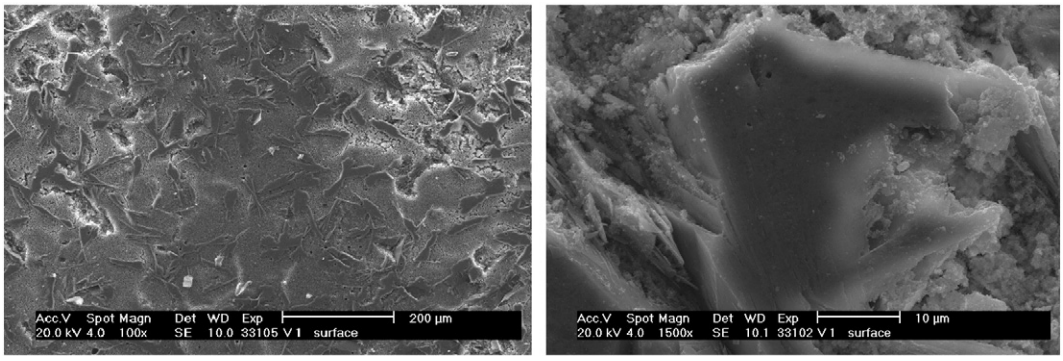

Fig. 18. SEM images of an upper surface of the sample mixed for 1 min.

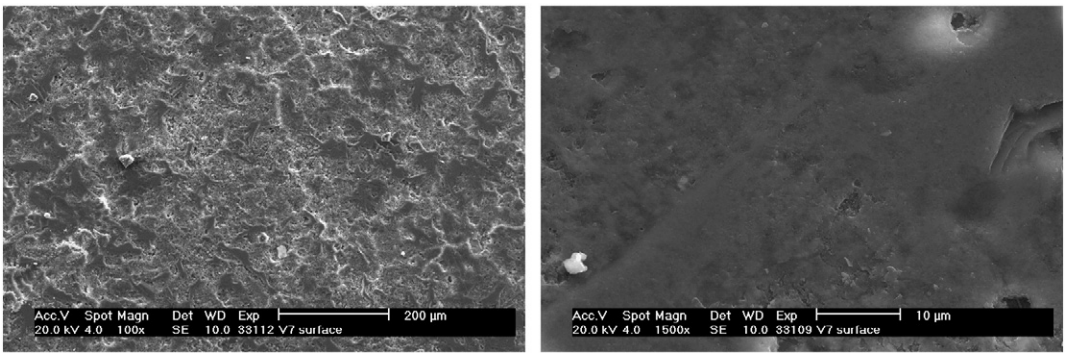

Fig. 19. SEM images of an upper surface of the sample mixed for 7 min.

5. Conclusions

In this study, the influences of different mixing energies on technological properties and hydration behaviour of grouting materials were studied on a laboratory scale. The following lists observations made and conclusions drawn:

Without changes in mortar composition and preparation (slurry A), as the mixing time period becomes longer,

- ➢ Fluidity worsens drastically. This holds true for flow values, as well as for efflux times
- ➢ Early shrinkage especially in the region of plastic shrinkage increases in drying conditions
- ➢ For sealed conditions there is almost no plastic shrinkage, but shrinkage as a result of massive hydration increases
- ➢ Setting times become shorter
- ➢ Early compressive strength increases.

These results can be explained by the following hypothesis:

- ➢ When an OPC-based grout containing super plasticizer is mixed, energy is introduced to the system. In the beginning this energy serves to produce homogeneous, well dispersed slurry. As more energy is introduced, slurry temperature increases, cement particles, early hydrates and adsorption of plasticizer are influenced.
- ➢ Longer mixing periods have an impact, in that new surfaces are created by either removing hydrates or superficial layers from cement grains or modifying the cement grains themselves. As a consequence, more plasticizer can be adsorbed. Further on in the hydration process, massive precipitation of hydrates occurs earlier — hydration is accelerated.
- ➢ If there are not enough plasticizer molecules dissolved in the water, part of the new surfaces will not be covered by plasticizer; hence flow values or workability decrease and plastic shrinkage increases. Accelerated hydration leads to shorter setting times, an increase in early strength and hydration induced shrinkage.
- ➢ If the original grout is overdosed with PCE, supplemental plasticizer can absorb on the new surfaces and workability is maintained. Acceleration of hydration as a function of introduced mixing energy still leads to the same effects described above. However, in contrast to slurry A with a lower dose of PCE, slurry B with a higher dose of PCE exhibited a measureable retardation of hydration.

Table 7
Chemical compositions using EDX on upper surfaces (Figs. 18 and 19) (mol%).

	Fig. 18	Fig. 19
CaO	95.6	78.4
SiO_2	2.3	15.0
SO_3	1.6	2.7
K_2O	0.4	1.8
Al_2O_3	0.2	1.4
Fe_2O_3	0.0	0.7

Further research is necessary in order to focus on quantifying the proposed influences of mixing energy on the dispersion of slurry and the subsequent structuring process. In particular, the effect of *activation of cement*, which is the creation of new active surfaces, needs to be investigated for fine powders that are widely used in cement and concrete mix design. Such studies that include mixes containing other additives such as super plasticizers based on naphthalenesulfonate, expansive additives and resin powders will play a decisive role in advancing understanding of the influences of mixing energy. Also, studies using saturated lime solution for mixing water could give more insight into the mechanisms of hydration acceleration.

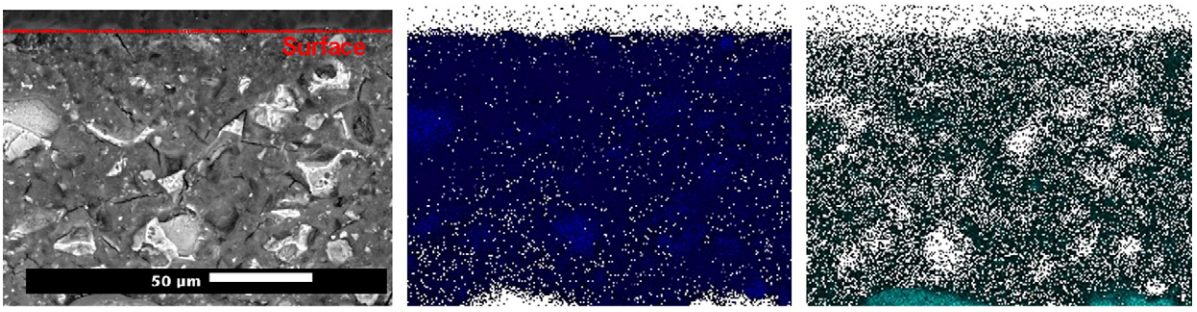

Fig. 20. Ca (center) and Si (right) mapping images of a cross section mixed for 1 min.

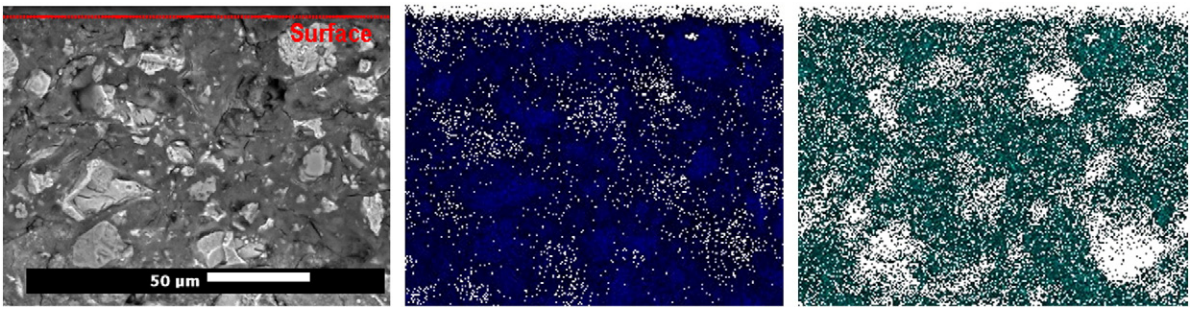

Fig. 21. Ca (center) and Si (right) mapping images of a cross section mixed for 7 min.

References

[1] K. Takahashi, Y. Hirano, M. Nukita, Development of Excellent Grouting Material in Fluidity and Crack Resistance, Proceeding of Architectural Institute of Japan, 2009, p. 1213.
[2] V. Fernandes, L. Silva, V.M. Ferreira, J.A. Labrincha, Evaluation of mixing and application process parameters of single-coat mortars, Cement and Concrete Research 35 (2005) 836–841.
[3] T. Sugiyama, T. Uomoto, Effect of chemical admixture on the strength development and micro-structure of mortar, Cement Science and Concrete Technology 57 (2003) 111–116.
[4] S. Martinez-Ramirez, F. Puertas, M.T. Blanco-Varela, G.E. Thompson, P. Almendros, Behaviour of repair lime mortars by wet deposition process, Cement and Concrete Research 28–2 (1998) 221–229.
[5] A. Baskoca, M.H. Ozkuli, S. Artirma, Effect of chemical admixtures on workability and strength properties of prolonged agitated concrete, Cement and Concrete Research 28–5 (1998) 737–747.
[6] K. Tsutsui, M. Ouchi, Change in flowability of self-compacting concrete due to pumping, Concrete Research and Technology 29 (2007) 79–84.
[7] J. Kuzel, Ein leistungsfähiges Wärmeleitungskalorimeter, TIZ-Fachberichte 108 (1) (1984).
[8] Friedrich W. Locher, Zement-Grundlagen der Herstellung und Verwendung, Vbt Verlag Bau U. Technik, Germany, 2000, pp. 205–206.
[9] K. Takahashi, Th. Bier, T. Westphal, Dynamics of phase development and shrinkage in cementitious systems, GDCh Monographie 42 (2010) 246–251.
[10] Y. Suto, T. Akiba, Cement Science Zatsuron, third ed., Japan cement association, Tokyo, 1999, pp. 15–20.
[11] I. Soroka, D. Ravina, Hot weather concreting with admixtures, Cement and Concrete Composite 20 (1998) 129.
[12] H.M. Jennings, P.L. Pratt, An experimental argument for the existence of a protective membrane surrounding portland cement during the induction period, Cement and Concrete Research 9 (1979) 501–506.
[13] E.M. Gartner, J.M. Gaidis, Hydration mechanisms, I, in: J. Skalny (Ed.), Materials Science of Concrete, Vol. 1, American Ceramic Society, Westerville, OH, 1989, pp. 95–125.
[14] J.W. Schweitzer, et al., In situ measurements of the cement hydration profile during the induction period, Proceedings of the Twelfth International Congress on the Chemistry of Cement, National Research Council of Canada, Montreal, Canada, 2007.
[15] J.W. Bullard, et al., Mechanisms of cement hydration, Cement and Concrete Research (in press), doi:10.1016/j.cemconres.2010.09.011.
[16] S. Garrault, A. Nonat, Hydrated layer formation on tricalcium and dicalcium silicate surfaces: experimental study and numerical simulations, Langmuir 17 (2001) 8131–8138.
[17] S. Garrault-Gauffinet, A. Nonat, Experimental investigation of calcium silicate hydrate (C–S–H) nucleation, Journal of Crystal Growth 200 (1999) 565–574.
[18] D. Damidot, A. Nonat, P. Barret, Kinetics of tricalcium silicate hydration in diluted suspensions by microcalorimetric measurements, Journal of the American Ceramic Society 73 (11) (1990) 3319–3322.
[19] J.P. Skalny, J.F. Young, Mechanisms of Portland Cement Hydration, 7th ISCC, 1980, II1/3–II1/45.
[20] P. Juilland, E. Gallucci, R. Flatt, K. Scrivener, Dissolution theory applied to the induction period in alite hydration, Cement and Concrete Research 40 (2010) 831–844.
[21] E.M. Gartner, J.F. Young, D.A. Damidot, I. Jawed, Hydration of portland cement, in: J. Bensted, P. Barnes (Eds.), Structure and Performance of Cements, 2nd Edition, Spon Press, New York, 2002, pp. 57–113.
[22] R. Holly, H. Peemoeller, et al., Magnetic resonance in situ study of tricalcium aluminate hydration in the presence of gypsum, Journal of the American Ceramic Society 89 (3) (2006) 1022–1027.
[23] J. Skalny, M.E. Tadros, Retardation of tricalcium aluminate hydration by sulfates, Journal of the American Ceramic Society 60 (3–4) (1977) 174–175.
[24] H. Minard, et al., Mechanisms and parameters controlling the tricalcium aluminate reactivity in the presence of gypsum, Cement and Concrete Research 37 (2007) 1418–1426.
[25] D. Dollimore, R.J. Mangabhai, Effect of mixing time on heat evolution pattern of cement pastes, Thermochimica Acta 85 (1985) 223–226.
[26] R. Ylmén, L. Wadsö, I. Panas, Insights into early hydration of Portland limestone cement from infrared spectroscopy and isothermal calorimetry, Cement and Concrete Composite 40 (2010) 1541–1546.
[27] S. Bishnoi, K.L. Scrivener, Studying nucleation and growth kinetics of alite hydration using μic, Cement and Concrete Research 39 (2009) 849–860.
[28] A. Hallal, et al., Combined effect of mineral admixtures with super plasticizers on the fluidity of the blended cement paste, Construction and Building Materials 24 (2010) 1418–1423.
[29] S. Hanehara, K. Yamada, Interaction between cement and chemical admixture from the point of cement hydration, absorption behaviour of admixture and paste rheology, Cement and Concrete Research 29 (1999) 1159–1165.
[30] D.J. Sun, et al., Effect of super plasticisers on adsorption, rate of cement hydration, and pore structure of cement pastes, Advances in Cement Research 21 (2009) 159–167.
[31] K. Yamada, et al., The adsorbing behaviour of polycarboxylate-type super plasticizer on cement hydrates and the effects of sulphate ion, Cement Science and Concrete Technology 55 (2002) 27–34.
[32] H. Kato, et al., Influence of temperature on the dispersion of cement particles by super plasticizers, Concrete Research and Technology 21 (2) (1999) 163–168.
[33] A.M. Neville, Properties of Concrete, third ed., Longman Scientific Technical, England, 1981, pp. 371–373.
[34] T.A. Bier, B. Stolte, Anwendung von Mortel und Beton mit Zeolith, 18, Steine-und-Erden-Kolloquium, 2009, pp. 43–52.
[35] A. Bentur, J.H. Kung, R.L. Berger, Effect of curing temperature on the pore structure of tricalcium silicate pastes, Journal of Colloid and Interface Science 74 (2) (1980) 549–560.